INTERNATIONAL JOURNAL OF PRECISION ENGINEERING AND MANUFACTURING-GREEN TECHNOLOGY Vol. 4, No. 2, pp. 221-226 APRIL 2017 / 221

REGULAR PAPER

DOI: 10.1007/s40684-017-0027-9
ISSN 2288-6206 (Print) / 2198-0810 (Online)

Fabrication of a SERS-Encoded Microfluidic Paper-Based Analytical Chip for the Point-of-Assay of Wastewater

Jae-Chul Lee[1,*], Wansun Kim[2,*], and Samjin Choi[1,2,#]

1 Department of Biomedical Engineering, College of Medicine, Kyung Hee University, 26, Kyungheedae-ro, Dongdaemun-gu, Seoul, 02447, South Korea
2 Department of Medical Engineering, Graduate School, Kyung Hee University, 26, Kyungheedae-ro, Dongdaemun-gu, Seoul, 02447, South Korea
Corresponding Author / E-mail: medchoi@khu.ac.kr, TEL: +82-2-961-0290, FAX: +82-2-961-5515
*Jae-Chul Lee and Wansun Kim contributed equally to this work

KEYWORDS: Gold nanoparticle, Wastewater, Surface-enhanced raman scattering, Successive ionic layer absorption and reaction technique, Paper chip

New environmental problems have arisen due to the production of numerous toxic materials with the development of industrial technologies. Although various technologies have been developed to solve these critical problems, the results were not satisfactory. Therefore, this study introduces a label-free, paper-based biosensing strip sensor to directly analyze the components of wastewater on site. Raman spectroscopy was used for fingerprinting the chemically-vibrational responses of the wastewater. In order to enhance the low signal intensity of the Raman results, the surface-enhanced Raman scattering (SERS) effect was implemented by using gold nanoparticles (AuNPs). Dense and uniform AuNPs were synthesized and distributed onto paper by a power-free successive ionic layer absorption and reaction (SILAR) method. The biosensing ability of the SERS paper strip showed a sensitivity of 10^{-10} M and an enhancement factor of 2.8×10^7 for rhodamine 6G. Two organic toxic drugs were selected to mimic wastewater. It was demonstrated that the SERS paper strip was sensitive to concentrations of 10^{-9} M and 10^{-5} M with correlation coefficients of 0.85 and 0.99 for 4-aminobenzoic acid and pyrocatechol, respectively. Therefore, the proposed SERS-encoded gold paper analytical strip has the potential to be used for the point-of-assay of wastewater.

Manuscript received: October 20, 2016 / Revised: January 17, 2017 / Accepted: February 14, 2017

1. Introduction

Water quality management is a challenging issue that is vital for human beings. Water-soluble pollutants, such as chlorides, nitrates, phosphates, and sulfates, are produced by product manufacturing or agricultural fertilizers and can cause eutrophication and asphyxia of aqueous ecosystems; thus, these materials must be specially managed.[1] In order to screen for these pollutants, which cause serious environmental problems, various monitoring methods (e.g., calorimetry, chromatography, UV spectrophotometry, and electric conductivity) have been used.[1-3] However, these are time-consuming and mono-anion detection methods that require pre-treatment process;[4] therefore, they are not so suitable for the continuous monitoring of water quality. Raman spectroscopy has been suggested as an alternative biosensing method to screen wastewater.

Raman spectroscopy is a direct, non-destructive analysis method that requires a small sample volume without additional preparation; thus, it is suitable for both *in-situ* and real-time measurements.[1] Basically, it is a spectroscopic technique used to measure the light scattered by the vibrational mode of a molecule. Unlike other spectroscopic methods, Raman spectroscopy provides a wide range of information related to the structure of a molecule.[5-9] Furthermore, it can be freely selected depending on the purpose of the desired wavelength of the laser that is used to irradiate to the molecule.[10-13] However, the low signal sensitivity of Raman spectroscopy is a critical drawback. To address this problem, the surface plasmon concentration phenomenon of metallic nanostructures has been used to enhance the sensitivity; this is referred to as surface-enhanced Raman scattering (SERS). In particular, when the frequency of an external light and the frequency of electrons in the nanostructured surface of a noble metal are resonated, the local electric field is concentrated. This phenomenon is referred to as surface plasmon resonance (SPR). A small area that possesses a concentrated electric field is called a hot spot. SPR is one of the causes of this SERS phenomenon.[14]

As a strategy to enhance the SERS phenomenon, most studies have focused on fabricating nanostructured and nanopatterned substrates. Most SERS-active substrates have been fabricated using complex and sophisticated methods that include lithography or high-temperature processes.[15] Alternatively, our research group suggested a low-cost, facile fabrication method to realize a SERS-encoded biosensing technique; this is referred to as successive ionic layer absorption and reaction (SILAR).[16-18] This paper-based fabrication method can achieve superior sensitivity and high reproducibility from biofluids. Therefore, in this paper, we attempted to expand this low-cost, fabrication-based screening method to analyze water quality (Scheme 1). Most sensor manufacturing technologies that are used for correct diagnosis and high-sensitivity detection utilize expensive equipment. Furthermore, most of the existing microfluidic chip-based biosensing devices used for fluid detection and control are complex, large in size, and expensive. Therefore, an alternative fabrication method is required for use in commercial environments and industries in order to reduce costs.[19] Recently, a microfluidic paper-based analytical device was studied in an attempt to overcome the disadvantages of current micro-device processing-based biosensor technologies.[20] Paper is inexpensive and it is easy to immobilize test samples using printing techniques. The introduced biofluids flow along hydrophilic channels via capillary action. They can be quantified by colorimetric methods without additional analyzing equipment.[21] However, the performance of quantification techniques based on colorimetry can be easily affected by a user's experience and the surrounding environment. Therefore, in our proposed strategy, we fabricate a paper-based device with SERS functionality using the SILAR technique. The ability of this SERS-encoded biosensing paper chip to screen wastewater is evaluated. Two organic toxic drugs, i.e., 4-aminobenzoic acid (PABA) and pyrocatechol, were selected to mimic wastewater. We believe that this low-cost, optical biosensing chip can also be expanded to other applications with no restrictions.

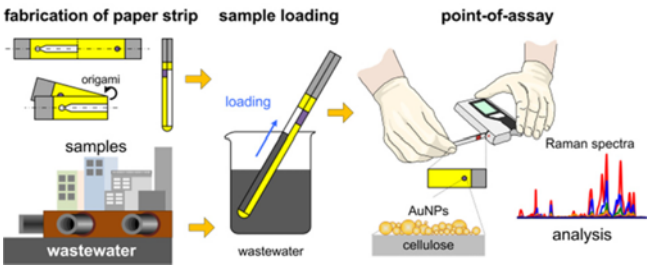

Scheme 1 Point-of-Assay for wastewater screening using a SILAR-fabricated, AuNP-evoked, SERS-encoded microfluidic paper chip, *SILAR: Successive ionic layer absorption and reaction, AuNP: Gold nanoparticle, SERS: Surface-Enhanced raman scattering

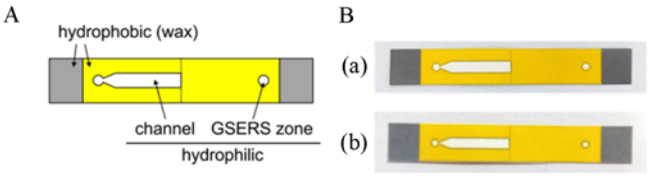

Fig. 1 (A) Design of the gold-deposited paper substrate and photos of (Ba) wax-treated, (B) Wax-and heat-treated paper substrates, GSERS: Gold SERS

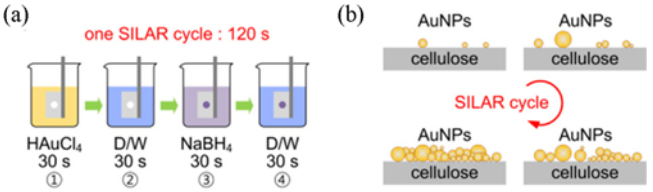

Fig. 2 The SILAR technique used to realize the AuNP-evoked SERS effect. (a) One SILAR cycle consisted of four successive steps including ① Treatment in a $HAuCl_4$ gold-containing solution, ② Washing with H_2O, ③ Treatment in a $NaBH_4$ reductant solution, ④ Rewashing with H_2O, (b) An increase in the number of SILAR cycles led to an increase in the size of AuNPs as well as a denser distribution of AuNPs

2. Material and Methods

2.1 Reagents

0.18-mm-thick Whatman® cellulose chromatography paper, gold (III) chloride trihydrate ($HAuCl_4$, > 99.9%), sodium borohydride ($NaBH_4$, > 96%), and rhodamine 6G (R6G, Raman probe) were used in this study. All reagents were of analytical grade, and all solutions were prepared using 18.3 $M\Omega \cdot cm^{-1}$ distilled water. All materials were purchased from Sigma Aldrich (St. Louis, MO, USA).

2.2 Fabrication of Paper Body

The designed paper substrate (Fig. 1(A)) consisted of hydrophilic and hydrophobic regions for the reactant path (wastewater) and barriers, respectively. The hydrophobic barriers were wax-printed by a Xerox ColorQube 8570 N printer (Fuji Xerox, Tokyo, Japan). In order to uniformly penetrate the inner paper, the wax-printed substrate was exposed to a temperature of 130°C in a drying oven for 45 s (Fig. 1(B)). The substrate was subsequently stored at room temperature.

2.3 Fabrication of SILAR-Synthesized GSERS Zone

The gold nanoparticles (AuNPs) were directly synthesized and grown on paper through the SILAR technique (Fig. 2), in which $HAuCl_4$ and $NaBH_4$ aqueous solutions were reacted through Eq. (1). The paper substrate was treated in a $HAuCl_4$ solution of gold ions and rinsed with water. It was then treated in a $NaBH_4$ reducing solution and rinsed with water to wash out any non-reacted residues. During each of these steps, the paper substrate was treated for 30 s; one SILAR cycle required a total of 120 s. The AuNPs were directly synthesized on the hydrophilic test zone, which is referred to as the GSERS zone.[16,17]

$$8HAUCl_4 + 3NaBH_4 + 6H_2O \rightarrow 8Au + 3NaBO_2 + 24HCL \quad (1)$$

2.4 Instrumentation

The morphology of AuNPs on the SERS paper strip was investigated using an S-4700 field emission scanning electron microscope (FE-SEM; Hitachi, Tokyo, Japan) at 5 kV. The size of AuNPs was analyzed using the ImageJ software (NIH, Bethesda, MD,

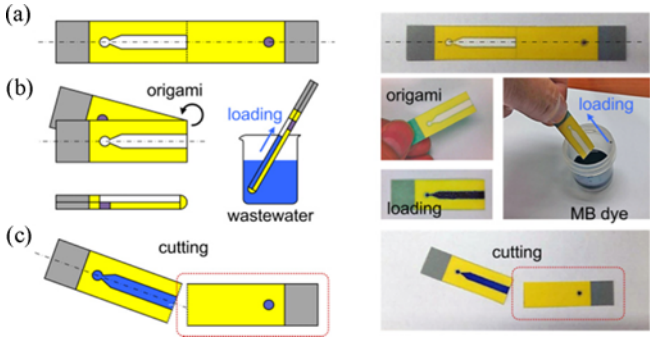

Fig. 3 Concepts and photos of SERS paper strip operation for real-time wastewater screening, Methylene blue (MB) water-soluble dye (Samchun pure chemical, seoul, korea) was used to color the water

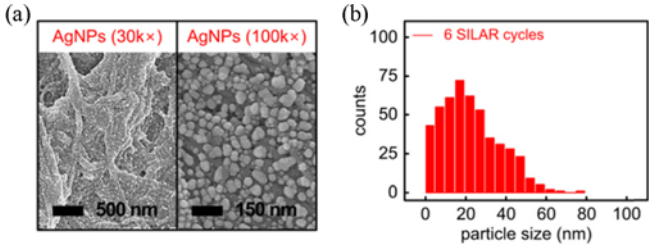

Fig. 4 (a) SEM photographs of the AuNPs synthesized under the optimal SILAR conditions on paper, (b) The size distribution of AuNPs

USA). The Raman spectra were obtained using a SENTERRA confocal Raman system (Bruker Optics, Billerica, MA, USA) by focusing a 785-nm diode laser source with 10 mW of power and a spot size of - 1.3 μm with a 50 × objective lens. All spectra were collected in the range of 417 - 1782 cm^{-1} with a spectral resolution of 5 cm^{-1} and twice the acquisition time of 10 s. Data were collected at 10 random points on the samples.

2.5 Numerical Analysis

The SERS effect of the nanostructure fabricated by the SILAR technique was theoretically evaluated using the finite element method (FEM). The FEM model was designed based on information about the AuNPs that was obtained from FE-SEM photographs and Gaussian fitting. The electric field distributions were analyzed according to the diameter of AuNPs, the diameter ratio, the gap distance between AuNPs, and the incident angle of the laser. This computational calculation was performed by the radiofrequency (RF) module of the COMSOL software.

3. Results and Discussion

3.1 Operation of SERS Paper Strip

Fig. 3(a) shows the concepts and photos of a SERS paper strip that is functionalized by SILAR-synthesized AuNPs in the GSERS zone. First, this device was folded in half along the dotted guide line (Fig. 3(b)). The folded SERS paper strip was then immersed in wastewater and the wastewater diffused via capillary action along the channel. Finally, the capillary-driven liquid was loaded onto the GSERS zone.[22] The channel part of the SERS paper strip was then cut (Fig. 3(c)), and the remaining SERS paper strip was used to screen the wastewater via mobile or benchtop Raman spectroscopy. Thus, this SERS strip can be used for quick analysis in point-of-care applications.

3.2 Characterization of SERS Paper Strip

Fig. 4(a) shows SEM photographs of the AuNPs synthesized by six SILAR cycles with 10 mM $HAuCl_4$ and $NaBH_4$ on paper. The AuNPs were synthesized by repeated sequential processes where the gold was absorbed and partially reduced, the excess reagents were eliminated by H_2O, the gold was fully reduced, and the non-reacted reagents and nonattached particles were eliminated. The presence of densely and uniformly distributed AuNPs deposited in the GSERS zone of the strip could be observed. Fig. 4(b) shows a graph indicating the particle size distribution, as estimated by the ImageJ software (NIH, Bethesda, MD, USA) from SEM photographs. The mean particle size of the synthesized AuNPs was 15 nm. The AuNPs were densely and homogeneously deposited onto the paper, which should lead to the presence of a strong SERS effect.

3.3 Numerical Analysis of SERS Paper Strip

Under the optimal SILAR conditions, the distributions of AuNP diameters and the mean gap distance between AuNPs were 6 - 60 nm and 6 nm, respectively. These values were used as references in the following analytical models to analyze a gold dimer. Three boundary conditions were used, including an active port boundary (for an incident wavelength boundary with an initial value of 1 W) and a passive port boundary (for a bottom boundary that does not pass reflections). The Floquet boundary condition was also imparted on both sides to provide an electric field with a symmetrical parallel boundary in the analysis models. The maximum and minimum finite element sizes for computational analysis were set at 1 nm and 0.002 nm, respectively. The material properties for the finite element analytical models were selected from the literature.[23,24] The refractive index of air was 1.000293 and the complex-valued permittivity of gold at 785 nm was - 15.0 - 0.9 *i*.

Fig. 5 shows the distribution of the maximum electric fields as a function of the incident angle of the laser for a AuNP with a diameter of 24 nm and a gap distance of 0.5 nm. The intensities of the maximum electric fields non-linearly decreased as the incident angle of the laser increased. Fig. 6 shows the changes in the maximum electric fields as a function of the gap distance between AuNPs. The range of gap distances was set from - 6 nm (overlapping AuNPs) to 6 nm. When the gap distance between two AuNPs was zero, the maximum electric field had the highest value (approximately 10^8). The intensities of the maximum electric fields logarithmically decreased as the gap distance between AuNPs increased. Fig. 7 shows the intensities of the maximum electric fields as a function of the AuNP size (from 6 nm to 60 nm). The intensities of the maximum electric fields linearly increased as the size of the AuNPs increased. Fig. 8 shows the changes in the maximum electric fields as a function of the size ratio between AuNPs. A diameter of 24 nm was used as a reference and the ratio was varied from 0.1 (24 nm versus 2.4 nm)

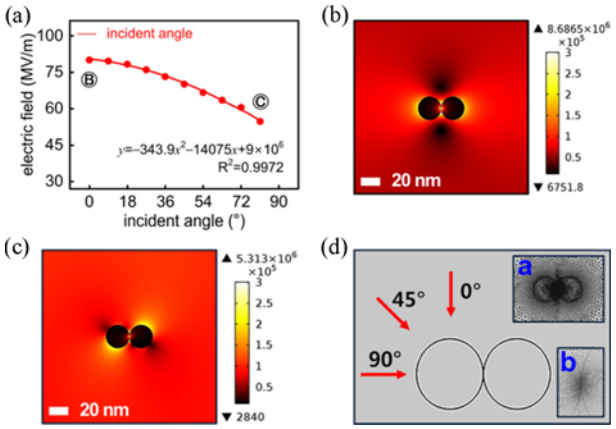

Fig. 5 (a) Effects of the incident laser angle on the distribution of the maximum electric fields for a gold dimer, Angles of (b) 0°, (c) 81°, (d) Concept used to evaluate the incident laser angles on the gold dimer

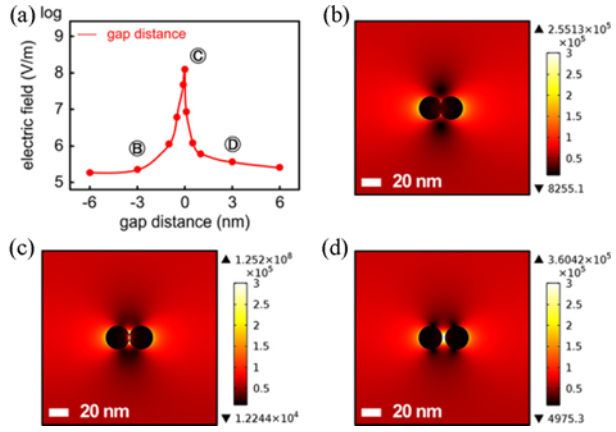

Fig. 6 (a) Effects of the gap distance between AuNPs on the distribution of the maximum electric fields for a gold dimer. Gap distances of (b) -3 nm, (c) 0 nm, (d) 3 nm

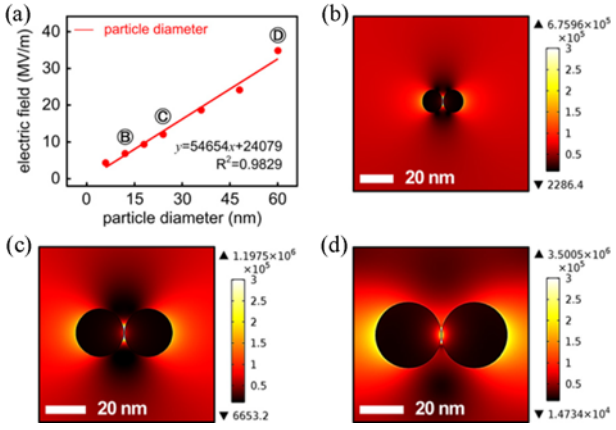

Fig. 7 (a) Effects of particle diameter on the distribution of the maximum electric fields for a gold dimer, Diameters of (b) 12 nm, (c) 24 nm, (d) 60 nm

to 2.5 (24 nm versus 72 nm). The intensities of the maximum electric fields non-linearly increased as the size ratio between AuNPs increased.

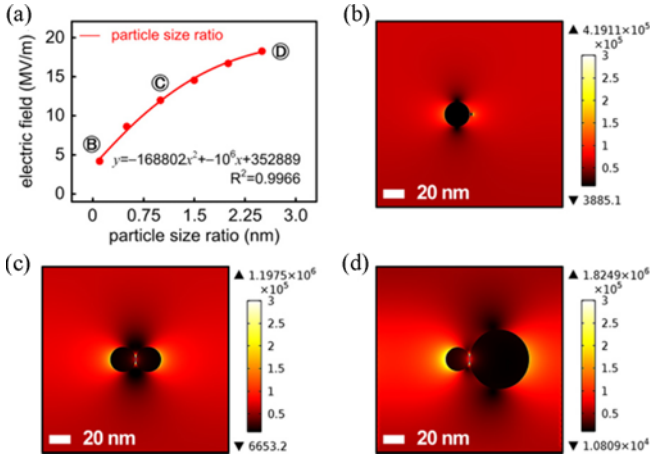

Fig. 8 (a) Effects of the ratio between particle sizes on the distribution of the maximum electric fields for a gold dimer, Ratios of (b) 0.1, (c) 1, (d) 2.5

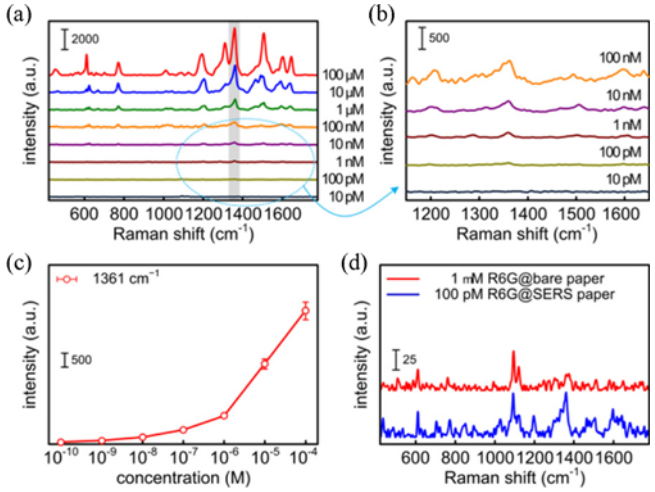

Fig. 9 Raman spectra with (a) Different R6G concentrations (10 pM - 100 μM), (b) Low concentrations of R6G on the SERS paper strip, (c) Variations in the Raman intensity at 1361 cm^{-1} with different R6G concentrations, (d) Raman spectra of R6G concentrations of 1 mM and 100 pM on the SERS and bare paper strips, respectively

3.4 SERS Activity

In order to quantify the SERS activity, the Raman intensities of different concentrations of R6G (10 pM to 100 μM, as shown in Fig. 9A) were evaluated. The R6G molecule showed dominant Raman peaks at 620 cm^{-1} (C - C ring) and at 1361 and 1647 cm^{-1} (C - C stretching).[25] The Raman peak at 1361 cm^{-1} was selected as the reference peak for the R6G molecule. The AuNP paper strip could clearly identify the presence of the R6G molecule at concentrations between 100 pM and 100 μM, but it could not detect the R6G molecule at concentrations less than 10 pM (Fig. 9(b)). Fig. 9(c) shows a plot of the Raman intensities of R6G from 100 pM to 100 μM at 1361 cm^{-1}; the correlation coefficient is 0.98. The enhancement factor (EF) of the SERS paper strip was calculated by[26]

$$EF = I_{SERS}/I_{bare} \times C_{bare}/C_{SERS}\,. \quad (2)$$

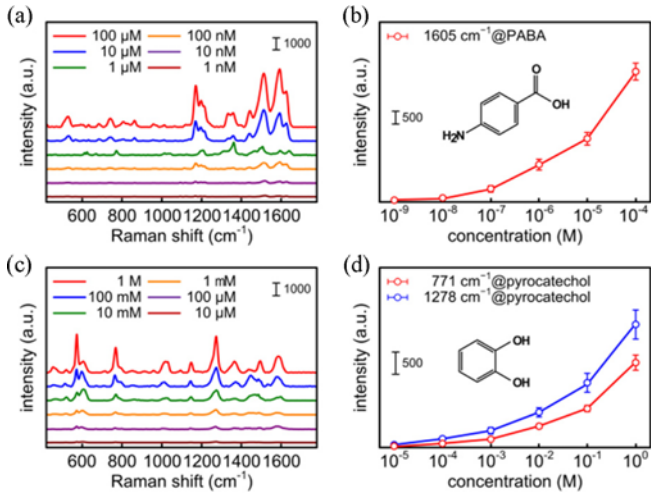

Fig. 10 Raman spectra with different concentrations of PABA ((a), 1 nM - 100 μM) and pyrocatechol ((c), 10 μM - 1 M), Variations in the Raman intensity (b) at 1605 cm^{-1} with PABA, (d) at 771 cm^{-1} and 1278 cm^{-1} with pyrocatechol; PABA: 4-Aminobenzonic acid

Here, C_{SERS} and C_{bare} are the concentrations of the R6G molecule on the SERS paper strip ($C_{SERS} = 10^{-10}$ M) and the bare paper ($C_{bare} = 10^{-3}$ M), respectively (Fig. 9(d)). The calculated SERS-EF was 2.8×10^7, where the Raman intensities of the SERS and bare paper strips at 1361 cm^{-1} were $I_{SERS} = 55.6$ and $I_{bare} = 19.7$, respectively. Therefore, the SERS paper strip is likely to have stable and superior performance for detecting the target molecules and determining their concentrations.

3.5 Bioapplication

The bioapplicability of the SERS paper strip was evaluated at different concentrations of PABA and pyrocatechol in attempts to detect the two organic toxic compounds. PABA has been used in biochemical, medical, and nutritional applications, but it may be hazardous to human health.[27] Fig. 10A shows the Raman spectra of different concentrations of PABA solutions (1 nM to 100 μM) on the SERS paper strip. Prominent peaks were observed at 1172 cm^{-1} and 1605 cm^{-1} (C - H ring stretching).[27,28] The Raman peak at 1605 cm^{-1} was selected as the marker of PABA, and its Raman intensity variations between concentrations of 1 nM and 100 μM had a correlation of 0.85 (Fig. 10(b)). Pyrocatechol is another toxic organic material that is used in pesticides and as a photographic developer. Fig. 10C shows the Raman spectra of different concentrations of pyrocatechol (10 μM to 1 M). Prominent peaks were observed at 771 cm^{-1} (C - C stretching) and 1278 cm^{-1} (O - H asymmetrical bending).[29] The variations of the Raman intensities for pyrocatechol between concentrations of 10 μM and 1 M had a correlation of 0.99 at 1278 cm^{-1} (Fig. 10(d)). The SERS paper strip showed high sensitivity for identifying these two organic toxic drugs. Therefore, the proposed SERS-encoded gold paper analytical strip has the potential to be used for the point-of-assay of wastewater.

4. Conclusions

This paper presented a SERS paper strip that could directly analyze the components of wastewater on site. This SERS paper strip was fabricated by using wax printing (to create a hydrophilic GSERS zone) and a SILAR technique (for AuNP deposition). Sample collection was performed with the origami process. The biosensing performance of the fabricated SERS paper strip was evaluated by a standard Raman probe (i.e., R6G) and confirmed with PABA (4-aminobenzonic acid) and pyrocatechol solutions. The R6G-induced SERS paper strip could measure concentrations as low as 10^{-10} M and had an SERS-EF of 2.8×10^7. When screening PABA and pyrocatechol solutions (used to simulate wastewater), the SERS paper strip achieved sensitivities of 10^{-9} M (with a correlation coefficient of 0.85) and 10^{-5} M (with a correlation coefficient of 0.99), respectively. The conventional indirect fabrication methods such as chemical synthesis of colloidal nanoparticles and centrifugal extraction require complicated processes for synthesizing and depositing nanoparticles on paper and result in the presence of aggregated nanoparticles showing non-uniform distribution of SERS region (AuNP or AgNP inks), while the proposed SERS paper strip can be fabricated by a low-cost, simple and facile method and yields superior sensitivity and high reproducibility. Therefore, the proposed AuNP-deposited SERS-encoded paper strip may be useful to quickly analyze wastewater on site; it could also be utilized for various other applications.

ACKNOWLEDGEMENT

This research was supported by a grant from the Korean Health Technology Research & Development Project, by the Ministry of Health & Welfare, Republic of Korea (HI14C2241).

REFERENCES

1. Mabrouk, K. B., Kauffmann, T., and Fontana, M., “Abilities of Raman Sensor to Probe Pollutants in Water,” Proc. of IOP Science in Journal of Physics: Conference Series, Vol. 450, No. 1, Paper No. 012014, 2013.
2. Miehe, R., Mueller, S., Schneider, R., Wahren, S., and Hornberger, M., “Integrated Hazardous Materials Management: Combining Requirements from Various Environmental Legislations to Enable Effective Business Compliance Processes in Industries,” Int. J. Precis. Eng. Manuf.-Green Tech., Vol. 2, No. 3, pp. 289-298, 2015.
3. Kang, H. S., Lee, J. Y., Choi, S., Kim, H., Park, J. H., et al., “Smart Manufacturing: Past Research, Present Findings, and Future Directions,” Int. J. Precis. Eng. Manuf.-Green Tech., Vol. 3, No. 1, pp. 111-128, 2016.
4. Lee, J.-I., Lee, J.-H., Lee, J.-H., Lee, J.-H., Lee, W.-S., et al., “Study on the Unification between KS I ISO Standard and Official Test Method Enacted by Korean Ministry of Environment-Drinking Water and Indoor Air Quality,” Analytical Science and Technology, Vol. 25, No. 2, pp. 102-113, 2012.
5. Choi, S., Moon, S. W., Shin, J.-H., Park, H.-K., and Jin, K.-H., “Label-Free Biochemical Analytic Method for the Early Detection

of Adenoviral Conjunctivitis Using Human Tear Biofluids," Analytical Chemistry, Vol. 86, No. 22, pp. 11093-11099, 2014.

6. Choi, S., Park, H. K., Min, G. E., and Kim, Y. H., "Biochemical Investigations of Human Papillomavirus-Infected Cervical Fluids," Microscopy Research and Technique, Vol. 78, No. 3, pp. 200-206, 2015.
7. Kim, Y. H., Chang, B., Choi, J. H., Park, H. K., and Choi, S., "Biochemical Fingerprints of Human Papillomavirus Infection and Cervical Dysplasia Using Cervical Fluids: Spectral Pattern Investigation," Microscopy Research and Technique, Vol. 79, No. 10, pp. 966-972, 2016.
8. Shin, J. H., Choi, J. H., Choi, S., Jung, G. B., Park, H. K., et al., "Clinico-Biochemical Investigations of Aging Effects on Normoglycemic and Hyperglycemic Murine Retinal Tissues," Microscopy Research and Technique, Vol. 77, No. 12, pp. 1023-1030, 2014.
9. Moon, S. W., Kim, W., Choi, S., and Shin, J. H., "Label-Free Optical Detection of Age-Related and Diabetic Oxidative Damage in Human Aqueous Humors," Microscopy Research and Technique, Vol. 79, No. 11, pp. 1050-1055, 2016.
10. Choi, S., Jung, G. B., Kim, K. S., Lee, G.-J., and Park, H.-K., "Medical Applications of Atomic Force Microscopy and Raman Spectroscopy," Journal of Nanoscience and Nanotechnology, Vol. 14, No. 1, pp. 71-97, 2014.
11. Zeng, S., Baillargeat, D., Ho, H.-P., and Yong, K.-T., "Nanomaterials Enhanced Surface Plasmon Resonance for Biological and Chemical Sensing Applications," Chemical Society Reviews, Vol. 43, No. 10, pp. 3426-3452, 2014
12. Polavarapu, L., Pérez-Juste, J., Xu, Q.-H., and Liz-Marzán, L. M., "Optical Sensing of Biological, Chemical and Ionic Species through Aggregation of Plasmonic Nanoparticles," Journal of Materials Chemistry C, Vol. 2, No. 36, pp. 7460-7476, 2014.
13. Liu, X., Shao, Y., Tang, Y., and Yao, K.-F., "Highly Uniform and Reproducible Surface Enhanced Raman Scattering on Air-Stable Metallic Glassy Nanowire Array," Scientific Reports, Vol. 4, p. 5835, 2014.
14. Cialla, D., März, A., Böhme, R., Theil, F., Weber, K., et al., "Surface-Enhanced Raman Spectroscopy (SERS): Progress and Trends," Analytical and Bioanalytical Chemistry, Vol. 403, No. 1, pp. 27-54, 2012.
15. Kim, W.-S., Shin, J.-H., Park, H.-K., and Choi, S., "A Low-Cost, Monometallic, Surface-Enhanced Raman Scattering-Functionalized Paper Platform for Spot-On Bioassays," Sensors and Actuators B: Chemical, Vol. 222, pp. 1112-1118, 2016.
16. Kim, W., Kim, Y.-H., Park, H.-K., and Choi, S., "Facile Fabrication of a Silver Nanoparticle Immersed, Surface-Enhanced Raman Scattering Imposed Paper Platform through Successive Ionic Layer Absorption and Reaction for On-Site Bioassays," ACS Applied Materials & Interfaces, Vol. 7, No. 50, pp. 27910-27917, 2015.
17. Kim, W., Lee, J.-C., Shin, J.-H., Jin, K.-H., Park, H.-K., et al., "Instrument-Free Synthesizable Fabrication of Label-Free Optical Biosensing Paper Strips for the Early Detection of Infectious Keratoconjunctivitides," Analytical Chemistry, Vol. 88, No. 10, pp. 5531-5537, 2016.
18. Lee, J.-C., Kim, W., Park, H.-K., and Choi, S., "Controlling Successive Ionic Layer Absorption and Reaction Cycles to Optimize Silver Nanoparticle-Induced Localized Surface Plasmon Resonance Effects on the Paper Strip," Spectrochimica Acta Part A: Molecular and Biomolecular Spectroscopy, Vol. 174, pp. 37-43, 2017.
19. Kim, J.-H., Shim, B. S., Kim, H. S., Lee, Y.-J., Min, S.-K., et al., "Review of Nanocellulose for Sustainable Future Materials," Int. J. Precis. Eng. Manuf.-Green Tech., Vol. 2, No. 2, pp. 197-213, 2015.
20. Martinez, A. W., Phillips, S. T., Whitesides, G. M., and Carrilho, E., "Diagnostics for the Developing World: Microfluidic Paper-Based Analytical Devices," ACS Publications, pp. 3-10, 2009.
21. Martinez, A. W., Phillips, S. T., Butte, M. J., and Whitesides, G. M., "Patterned Paper as a Platform for Inexpensive, Low-Volume, Portable Bioassays," Angewandte Chemie International Edition, Vol. 46, No. 8, pp. 1318-1320, 2007.
22. Choi, S., Kim, S.-K., Lee, G.-J., and Park, H.-K., "Paper-Based 3D Microfluidic Device for Multiple Bioassays," Sensors and Actuators B: Chemical, Vol. 219, pp. 245-250, 2015.
23. Bakker, J., Bryntse, G., and Arwin, H., "Determination of Refractive Index of Printed and Unprinted Paper Using Spectroscopic Ellipsometry," Thin Solid Films, Vol. 455, pp. 361-365, 2004.
24. Foo, K. L., Hashim, U., Muhammad, K., and Voon, C. H., "Sol-Gel Synthesized Zinc Oxide Nanorods and their Structural and Optical Investigation for Optoelectronic Application," Nanoscale Research Letters, Vol. 9, No. 1, pp. 429, 2014.
25. Zhao, Y., Tian, Y., Ma, P., Yu, A., Zhang, H., et al., "Determination of Melamine and Malachite Green by Surface-Enhanced Raman Scattering Spectroscopy Using Starch-Coated Silver Nanoparticles as Substrates," Analytical Methods, Vol. 7, No. 19, pp. 8116-8122, 2015.
26. Le Ru, E., Blackie, E., Meyer, M., and Etchegoin, P. G., "Surface Enhanced Raman Scattering Enhancement Factors: A Comprehensive Study," The Journal of Physical Chemistry C, Vol. 111, No. 37, pp. 13794-13803, 2007.
27. Qu, L.-L., Song, Q.-X., Li, Y.-T., Peng, M.-P., Li, D.-W., et al., "Fabrication of Bimetallic Microfluidic Surface-Enhanced Raman Scattering Sensors on Paper by Screen Printing," Analytica Chimica Acta, Vol. 792, pp. 86-92, 2013.
28. Suh, J., Di Lella, D., and Moskovits, M., "Surface-Enhanced Raman Spectroscopy of Colloidal Metal Systems: A Two-Dimensional Phase Equilibrium in P-Aminobenzoic Acid Adsorbed on Silver," The Journal of Physical Chemistry, Vol. 87, No. 9, pp. 1540-1544, 1983.
29. Navarrete, J. L. and Ramírez, F., "A Study by Raman Spectroscopy and the Semiempirical AM1 Method on Several 1, 2-Dihydroxybenzene Solutions," Spectrochimica Acta Part A: Molecular Spectroscopy, Vol. 49, No. 12, pp. 1759-1767, 1993.